Supplementary Material

Supplementary Tables

Table S1. Physicochemical properties of the ZEBRA CPP truncations

ZEBRA CPP only				
CPP	Residues	pI	Aliphatic index	Hydropathicity (GRAVY)
Z12	42	11.06	81.43	-1.095
Z13	42	11.38	81.43	-1.174
Z14	30	11.5	62	-1.32
Z15	17	12	28.8	-1.96
Z16	15	5.45	39.3	-1.493
Z17	13	8.6	105.38	-0.477
Z18	19	9.98	113.16	-0.637
Z19	8	11.1	48.75	-1.95
Z20	11	12	44.75	-1.64

Table S2. Physicochemical properties of the ZEBRA CPP truncations conjugated to OVACD8 cargo

ZEBRA CPP conjugated to OVACD8 cargo				
CPP	Residues	pI	Aliphatic index	Hydropathicity (GRAVY)
Z12	58	10.17	85.86	-0.941
Z13	58	10.34	85.86	-0.998
Z14	46	10.28	74.35	-1.046
Z15	33	10.37	62.12	-1.270
Z16	31	4.54	69.35	-1.00
Z17	29	5.02	101.03	-0.510
Z18	35	5.19	106	-0.591
Z19	24	8.43	81.25	-1.008
Z20	27	9.52	75.93	-0.752

Table S3. Physicochemical properties of the ZEBRA CPP truncations conjugated to MART1 cargo

ZEBRA CPP conjugated to MART1 cargo				
CPP	Residues	pI	Aliphatic index	Hydropathicity (GRAVY)
Z13	60	10.75	109	-0.378
Z14	48	10.73	103.75	-0.269
Z15	35	11.10	103.14	-0.191
Z18	37	6.31	142.43	0.392
Scramble	35	4.87	134	0.649

Table S4. Physicochemical properties of the ZEBRA CPP truncations conjugated to OVACD8CD4 cargo

ZEBRA CPP conjugated to OVACD8CD4 cargo				
CPP	Residues	pI	Aliphatic index	Hydropathicity (GRAVY)
Z13	83	9.91	90.6	-0.743
Z14	71	9.82	83.94	-0.731
Z15	58	9.77	79.14	-0.788
Z18	60	5.29	104.17	-0.408

Table S5. Physicochemical properties of the ZEBRA CPP truncations conjugated to OVACD4gp100CD8 cargo

ZEBRA CPP conjugated to OVACD4gp100CD8 cargo				
CPP	Residues	pI	Aliphatic index	Hydropathicity (GRAVY)
Z13	84	10.78	91.79	-0.707
Z14	72	10.77	85.42	-0.689
Z18	61	9.52	105.57	-0.364

Supplementary Figure legends

Figure S1. Design of eight variants (Z13 to Z20) based on truncations of ZEBRA CPP Z12. First and last amino acid is shown (single letter amino acid code) with the corresponding position on complete ZEBRA CPP.

Figure S2. Correlation graphs between CPP variant theoretical pI value and in vitro results. (A) Transduction was assessed in human DCs. Cells were incubated for 4h with the fluorescein-conjugated constructs (Z13OVACD8FAM, Z14OVACD8FAM, Z15OVACD8FAM or Z18OVACD8FAM) then subjected to a 30 sec wash with an acidic buffer to remove membrane bound peptide before FACS analysis. Correlation between CPP variant theoretical pI value and the percentage of transduced cells (n=3 for each CPP variant). Pearson correlation coefficient r=0.8668. Solid line and dashed lines represent regression line and 95% confidence bands, respectively (p=0.0003). (B) Correlation between CPP variant theoretical pI value and the percentage of IFN-γ-producing CD8 T cells. Pearson correlation coefficient r=0.9403. Solid line and dashed lines represent regression line and 95% confidence bands, respectively (p=0.0173).

Figure S3. CD8 and CD4 T cell immune responses elicited by vaccination with ZEBRA CPP truncations combined to TLR3 agonist (Hiltonol). Mice were vaccinated three times (wk0, wk2 and wk9) by s.c. injection of 10 nmoles of OVACD8CD4 (the cargo without ZEBRA CPP truncation), Z13OVACD8CD4, Z14OVACD8CD4, Z15OVACD8CD4, Z18OVACD8CD4 and i.m. injection of 50 µg of Hiltonol. One week after the last vaccination, mice were bled for assessing $OVA_{257-264}$-specific CD8 T cells by FACS multimer staining (A). Intracellular staining assay was performed on spleen cells for detecting multifunctional CD8 T cells (B) or CD4 T cells (C) after 6h stimulation with $OVA_{257-264}$ peptide or $OVA_{323-339}$ peptide respectively. Percentage of CD8 or CD4 T cells positive for each cytokine pattern is indicated *, $p<0.05$.

Figure S4. CD8 and CD4 T cell immune responses elicited by vaccination with ZEBRA CPP truncations combined to TLR2 agonist (Pam3CSK4) or TLR4 (MPLA). Mice were vaccinated three times (wk0, wk2 and wk9) by s.c. injection of 10 nmoles of OVACD8CD4 (the cargo without ZEBRA CPP truncation), Z13OVACD8CD4, Z14OVACD8CD4, Z15OVACD8CD4 or Z18OVACD8CD4 and 20 µg of Pam3CSK4 (A) or 20 µg of MPLA

(B). One week after the last vaccination, mice were bled for assessing $OVA_{257-264}$-specific CD8 T cells by FACS multimer staining. *, $p<0.05$; **, $p<0.01$.

Figure S5. Effect of Z13Trp2 on control of melanoma lung metastasis growth. Mice were implanted i.v. with $1x10^5$ B16-OVA melanoma tumor cells and vaccinated three times (d-21, d-7 and d7) by subcutaneous injection of 2nmoles of Z13Trp2 mixed with 100 μg of anti-CD40 and by i.m. injection of 50 μg of Hiltonol (right hind leg). Control mice group received anti-CD40 and hiltonol. Mice were euthanized at day 14 and lung recovered. Number of metastasis foci was counted for each lung (5 to 8 mice / group). Two representative lung pictures of each group are shown **, $p<0.01$ (Mann-Whitney test).

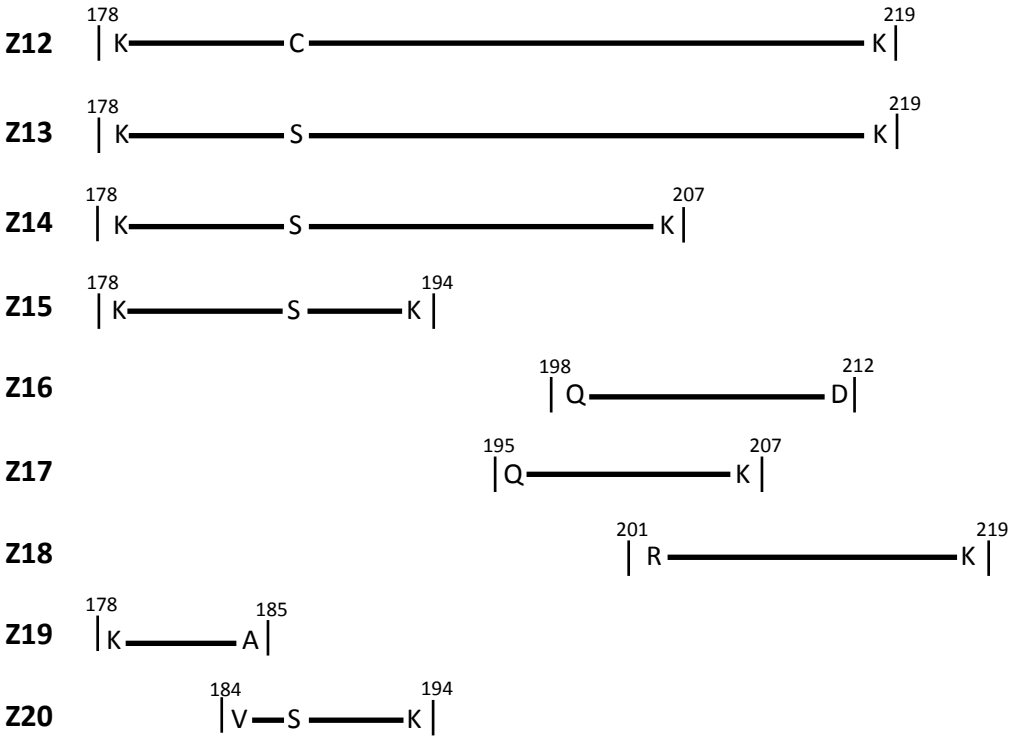
Z12
178
K
C
219
K
Z13
178
K
S
219
K
Z14
178
K
S
207
K
Z15
178
K
S
194
K
Z16
198
Q
212
D
Z17
195
Q
207
K
Z18
201
R
219
K
Z19
178
K
185
A
Z20
184
V
S
194
K

Figure S1

A

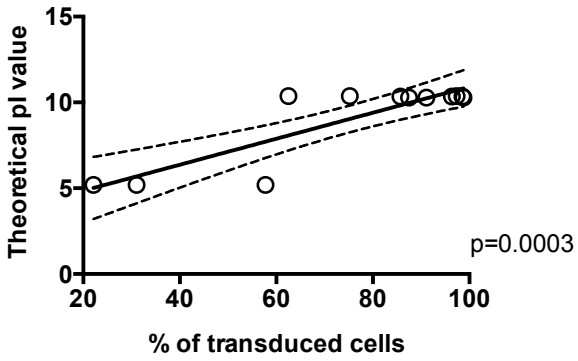
Theoretical pI value
15
10
5
0
20
40
60
80
100
% of transduced cells
p=0.0003

B

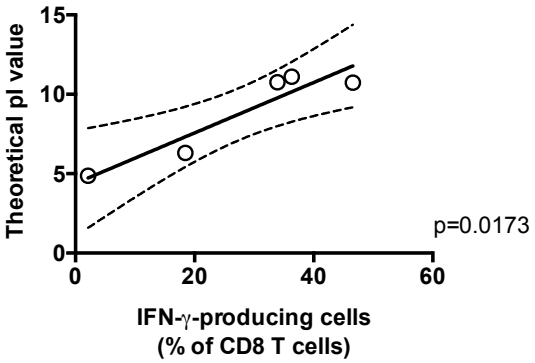
Theoretical pI value
15
10
5
0
0
20
40
60
IFN-γ-producing cells
(% of CD8 T cells)
p=0.0173

Figure S2

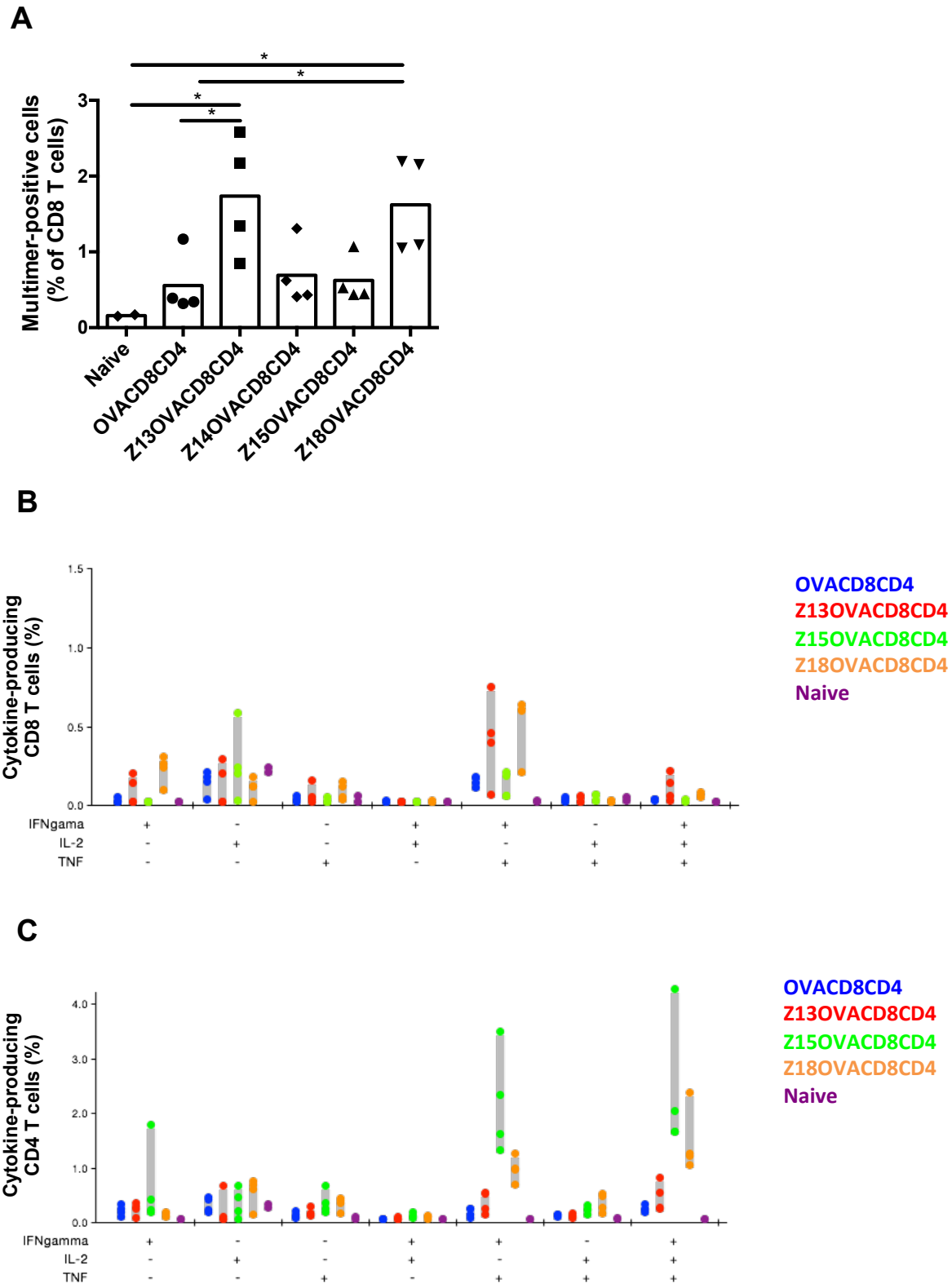
A
Multimer-positive cells (% of CD8 T cells)
Naive
OVACD8CD4
Z13OVACD8CD4
Z14OVACD8CD4
Z15OVACD8CD4
Z18OVACD8CD4
B
Cytokine-producing CD8 T cells (%)
IFNgama
IL-2
TNF
OVACD8CD4
Z13OVACD8CD4
Z15OVACD8CD4
Z18OVACD8CD4
Naive
C
Cytokine-producing CD4 T cells (%)
IFNgamma
IL-2
TNF
OVACD8CD4
Z13OVACD8CD4
Z15OVACD8CD4
Z18OVACD8CD4
Naive

Figure S3

A

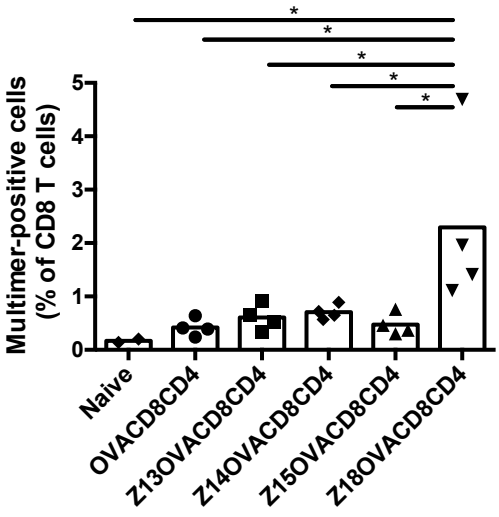
Multimer-positive cells
(% of CD8 T cells)
0
1
2
3
4
5
*
*
*
*
*
Naive
OVACD8CD4
Z13OVACD8CD4
Z14OVACD8CD4
Z15OVACD8CD4
Z18OVACD8CD4

B

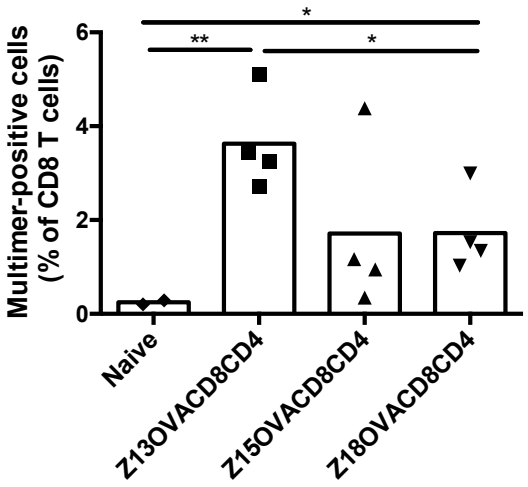
Multimer-positive cells
(% of CD8 T cells)
0
2
4
6
*
**
*
Naive
Z13OVACD8CD4
Z15OVACD8CD4
Z18OVACD8CD4

Figure S4

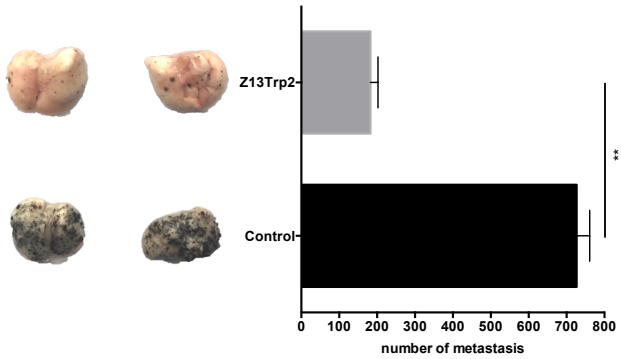
Z13Trp2
Control
**
0
100
200
300
400
500
600
700
800
number of metastasis

Figure S5